Hindawi
Advances in Civil Engineering
Volume 2023, Article ID 8703610, 10 pages
https://doi.org/10.1155/2023/8703610

Research Article

Critical State-Based Mohr–Coulomb Bounding Surface Model for Sand under Monotonic Shearing

Sang Inn Woo

Department of Civil and Environmental Engineering, Incheon National University, Yeonsu-gu, Incheon 20122, Republic of Korea

Correspondence should be addressed to Sang Inn Woo; siwoo@inu.ac.kr

Received 19 July 2022; Revised 12 March 2023; Accepted 15 March 2023; Published 4 April 2023

Academic Editor: Bingxiang Yuan

This study proposes a new constitutive model to describe the smooth transition from an elastic to a plastic response in sands under monotonic shearing. The model modifies the conventional Mohr–Coulomb model by considering the concept of a bounding surface and critical state soil mechanics. The friction angle consists of the critical state friction angle and a portion of the dilatancy angle, which is determined from the distance to the critical state line. Incorporating the bounding surface and the dilatancy angle into constitutive relationships for Toyoura sand produces numerical simulation results that have good agreement with the experimental results.

1. Introduction

The Mohr–Coulomb (M-C) model, with the accompanying nonassociated flow rule, is one of the most widely used constitutive models for describing the behavior of pressure-sensitive frictional materials, such as sands. In a conventional soil M-C model, the friction and dilatancy angles (ϕ_b and ϕ_d, respectively) are generally assumed to be constants during shearing. However, keeping them constant during the entire shearing process violates a fundamental and widely accepted principle of critical state soil mechanics that the density and stress states of sand eventually stabilize at the critical state. Accordingly, the conventional M-C model suffers from several limitations, such as an inability to describe the peak behavior of dilative sands under drained conditions and incorrectly simulating undrained stress-strain responses in sands.

Recently, geotechnical construction projects have been related to ground reinforcement with untraditional materials (i.e., glass fiber) [1, 2] or the geotechnical structures (i.e., piles) subjected to the cyclic loading conditions [3, 4]. To describe these situations more realistically, the more complex and rigorous soil constitutive model is required. Accordingly, Bai et al. [5] and Bai et al. [6] proposed constitutive models based on soil particle rearrangement within the framework of the granular thermodynamics to describe the thermomechanical responses of ground.

On the other hand, a critical state-based, refined version of the M-C model for sands was proposed by Woo et al. [7]. This study improves their critical state-based Mohr–Coulomb (CSMC) model by leveraging the concept of bounding surface plasticity. In the study by Woo et al. [7], the dilatancy angle of sand was proposed as a function of the state parameter ψ_c [8], with reference to the critical state theory [9] and careful observation of dilatancy [10]. By following the concept proposed by Wood et al. [11], Woo et al. [7] also decomposed the total friction angle into fractions of the critical state friction angle ϕ_c, which is a material constant that depends on the intrinsic properties of sand, and the dilatancy angle, which is a function of ψ_c.

The CSMC model [7] can simulate sand mechanical responses that conform to critical state soil mechanics, such as convergence to the critical state, as well as describe the peak behavior in dilative sands. However, the model exhibits piecewise continuous stress-strain responses (e.g., the kink at the peak under drained shearing for dilative sands) and overestimates the stiffness of sands at early loading stages. These shortcomings are primarily attributed to the use of a yield surface, which sharply distinguishes between elastic and plastic regions in a stress space. Bounding surface

models have successfully described the smooth (and more realistic) stress-strain relationships in soil by applying a tiny yield surface [12–16] or one without a yield surface [17–20] inside the bounding surface that corresponds to the failure surface in the stress space. Accordingly, this study proposed a bounding surface critical state-based Mohr–Coulomb (BSCSMC) model for sands to simulate a smooth transition from an elastic to a plastic response while retaining the advantages of the CSMC model.

2. Model Formulation

2.1. Mathematical Expression of Critical State (Steady State) of Sand. The critical state [9] describes the condition in a saturated soil after prolonged shearing, and it is mathematically expressed as follows [21]:

$$\begin{aligned} \frac{\partial p'}{\partial t} &= 0, \\ \frac{\partial q}{\partial t} &= 0, \\ \frac{\partial V}{\partial t} &= 0, \\ \frac{\partial \varepsilon_q}{\partial t} &\neq 0, \end{aligned} \tag{1}$$

where t is the time; p' is the mean effective stress; $(=\sigma_{kk}'/3)$, $q(=(3J_2)^{(1/2)})$ is the von Mises stress, where J_2 is the second invariant of a deviatoric stress $s_{ij} = (\sigma_{ij}' - p'\delta_{ij})$; V is the volume; and ε_q is the shear strain. According to equation (1), V, q, and p' are the constants at the critical state; therefore, they can be used for mathematically quantifying the critical state.

In this study, the projection of the critical state on the stress space (i.e., p'-q plane) is defined as the critical state surface (CSS), which have been generally assumed to be a linear function in the p'-q plane:

$$q = M_c(\theta)p', \tag{2}$$

where M_c is the critical state stress ratio $(=q/p')$ that is a function of the Lode's angle θ, which represents a deviatoric loading direction. In this study, Lode's angle θ is the defined as

$$\theta = \frac{1}{3}\sin^{-1}\left(\frac{3\sqrt{3}}{2}\frac{J_3}{J_2^{(3/2)}}\right), \tag{3}$$

where J_3 is the determinant of deviatoric stress. In equation (3), $\theta = 30^\circ$ and -30° under triaxial compression and extension conditions, respectively.

In the plane of volume (or void ratio e) and mean effective stress p', the locus of the critical state is termed as the critical state line (CSL). Li [22] suggested a mathematical expression for the CSL of sands based on the triaxial experimental data from Verdugo and Ishihara [23] as follows:

$$e_c = \Gamma_c(\theta) - \lambda\left(\frac{p'}{p_a}\right)^{\xi}, \tag{4}$$

where e_c is the critical state void ratio, Γ_c is e_c at $p' = 0$, p_a is a reference pressure (≈100 kPa), and λ and ξ are the positive material constants. Yoshimine et al. [24] reported that CSL depends on the loading directions. To reflect this dependency, this model assumes the intercept Γ_c of CSL as a function of Lode's angle θ:

$$\Gamma_c(\theta) = \left(\frac{\Gamma_{cc} + \Gamma_{ce}}{2}\right) + \left(\frac{\Gamma_{cc} - \Gamma_{ce}}{2}\right)\sin\theta, \tag{5}$$

where Γ_{cc} and Γ_{ce} are Γ_c under triaxial compression and extension conditions, respectively.

The critical state is a good reference state for the destination of mechanical responses of soil upon shearing; to quantify how far the current state of sand locates to the critical state, state parameters [8, 10, 25] have been proposed, as reviewed by Lashkari [25]. To define the current e-p' state with respect to the critical state, this study adopted the state parameter ψ_c proposed by Been and Jefferies [8], which is obtained by subtracting the critical state void ratio e_c from the current void ratio e.

$$\psi_c = e - e_c. \tag{6}$$

2.2. Friction Angles as a Function of the Dilatancy Angle. Theoretical and experimental studies [10, 26, 27] have suggested that the dilatancy angle is not constant, rather, it changes during shearing. Accordingly, Woo et al. [7] proposed a mathematical expression for dilatancy angle ϕ_d as

$$\phi_d = -d_0\psi_c, \tag{7}$$

where d_0 is a positive material constant. The dilatancy angle ϕ_d obtained from equation (7) is positive for dilative sand $(\psi_c < 0)$ and negative for contractive sand $(\psi_c > 0)$. At the critical state $(\psi_c = 0)$, the dilatancy angle ϕ_d becomes zero according to equation (7).

In the present model, to simulate the peak in the stress-strain response of dense (or dilative) sands, the friction angle ϕ_b is defined as a function of the state parameter based on Bolton's theory [10]:

$$\phi_b = \phi_c - 0.8d_0\psi_c, \tag{8}$$

where ϕ_c is the critical state friction angle. For dense (or dilative) sand $(\psi_c < 0)$, eq. (8) yields $\phi_b > \phi_c$, which allows the proposed model to describe peak behavior. At the critical state $(\psi_c = 0$ and $\phi_d = 0)$, ϕ_b is identical to ϕ_c, as given by equation (8).

2.3. Elastic Moduli. In the proposed model, the elastic response of sands is described by the tangential shear and bulk moduli. Herein, following Richart et al. [28], the maximum (or small strain) shear modulus G_0 is a function of e and p':

$$G_0 = C_g \frac{(2.97 - e)^2}{1 + e} \sqrt{p' p_a}, \tag{9}$$

where C_g is a positive material constant. To model the nonlinear elasticity of sand, previous studies [13, 14, 29, 30] suggested using the degradation function T to compute the tangential shear modulus as $G = G_0/T$. For monotonic shearing, Papadimitriou and Bouckovalas [30] defined T as

$$T = 1 + 2\left(\frac{1}{\alpha} - 1\right) \min\left[\frac{\sqrt{(1/2)(\mathbf{r} - \mathbf{r}_i) : (\mathbf{r} - \mathbf{r}_i)}}{2\alpha (G_{0i}/p_i')\gamma_{tv}}, 1.0\right], \tag{10}$$

where α is a material constant between zero to one, p_i' is the initial p', G_{0i} is the initial G_0, and γ_{tv} is the volumetric threshold strain. Herein, the tangential bulk modulus K is computed from the tangential shear modulus G and Poisson's ratio ν based on elasticity theory as follows:

$$K = \frac{2(1 + \nu)}{3(1 - 2\nu)} G. \tag{11}$$

The main limitation of equations (9) to (11) in the construction of elastic moduli is that they are purely empirical and based on the hypoelastic formulation; thus, the elastic pair used in this study cannot guarantee the conservation of energy in closed loop stress strain paths, as investigated by Einav et al. [31] and Lashkari and Golchin [32].

2.4. Bounding Surface, Mapping Rule, and Hardening Rule. The present model uses the rounded M-C failure surface [33] as its bounding surface:

$$f = \sqrt{J_2} K_f(\theta) - p' \sin\phi_b = 0, \tag{12}$$

where K_f is a function of Lode's angle θ, which makes corners of the bounding surface smooth. Following equation (3), at the corners of the M-C failure surface, Lode's angle θ is equal to 30° and −30° under triaxial compression and extension conditions, respectively. Abbo [33] used the limit Lode's angle θ_T (of which the value is closed to θ at the corner of the M-C failure surface) to build a smoothed M-C failure surface. When the absolute value of θ is less than the limit Lode's angle θ_T, the function K_f is defined by

$$K_f = \cos\theta - \frac{1}{\sqrt{3}} \sin\phi \sin\theta. \tag{13}$$

If $|\theta| > \theta_T$ (near the corners of the M-C failure surface), the function K_f has the following form:

$$K_f = A - B \sin 3\theta, \tag{14}$$

where functions A and B are defined by

$$A = \left[\cos\theta_T + \frac{1}{3}\cos\theta_T \tan\theta_T \tan 3\theta_T\right] + \left[\frac{1}{3\sqrt{3}}\cos\theta_T (\tan 3\theta_T - 3\tan\theta_T)\right] \text{sign}(\theta) \sin\varphi, \tag{15}$$

$$B = \frac{\sqrt{3}}{9} \frac{\cos\theta_T}{\cos 3\theta_T} \sin\phi + \frac{1}{3} \frac{\sin\theta_T}{\cos 3\theta_T} \text{sign}(\theta). \tag{16}$$

Equations (12)–(16) are combined to realize the M-C failure surface with smooth corners, which is used as a bounding surface in this study. Furthermore, the limit Lode angle θ_T is set as 29° to smooth the corners of the bounding surface without losing its stress anisotropy. By combining equation (12) and the relationship $q = (3J_2)^{1/2}$, the stress ratio M_b at the bounding surface can be written as

$$M_b(\theta) = \frac{\sqrt{3} \sin\phi_b}{K_f}. \tag{17}$$

Figure 1 shows the bounding surface of the present model in the π plane of normalized deviatoric stress $\mathbf{r}$ ($= \mathbf{s}/p'$) together with the mapping rule applied in this study, partially following Li and Dafalias [18]. In Figure 1, $\mathbf{r}_i$ is the initial **r,** and **n**, representing the shearing direction, is defined by

$$\mathbf{n} = \frac{\mathbf{r} - \mathbf{r}_i}{\rho}, \tag{18}$$

where ρ represents the tensorial distance between $\mathbf{r}$ and $\mathbf{r}_i$:

$$\rho = \sqrt{(\mathbf{r} - \mathbf{r}_i) : (\mathbf{r} - \mathbf{r}_i)}. \tag{19}$$

In the present model, modified from Li and Dafalias [18], hardening modulus H is defined as

$$H = \sqrt{\frac{2}{3}} G h_0 \frac{\rho_b}{\rho}, \tag{20}$$

where h_0 is a positive material constant and the function ρ_b is defined by

$$\rho_b = \sqrt{\frac{2}{3}} M_b - \mathbf{r} : \mathbf{n}, \tag{21}$$

which represents the distance to the bounding surface from the current state. In equation (20), the shear modulus G (obtained from equations (9) and (10)) indicates the effect of volume (or void ratio e) and confinement (p') on H. At the onset of shearing, $H = \infty$ because $\mathbf{r} = \mathbf{r}_i$, and $\rho = 0$; thus, the

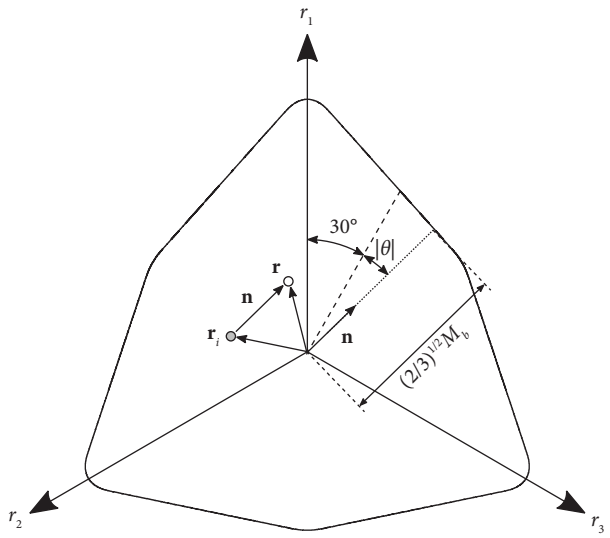

Figure 1: Mohr–Coulomb bounding surface and mapping rule.

model fully describes the elastic behavior of sand upon initial shearing. If **r** is inside the bounding surface, $\rho_b > 0$ and $H > 0$; thus, **r** moves outward to the bounding surface. If the current r is located outside the bounding surface, $\rho_b < 0$ and $H < 0$; therefore, **r** travels inward to the bounding surface. In summary, stress always evolves toward the bounding surface. Equation (17) demonstrates that the bounding surface eventually converges to the CSS because $\phi_d = 0$ and $\phi_b = \phi_c$ at the critical state.

The present model relies on the nonassociated flow rule; the direction of the plastic strain is proportional to the gradient of plastic potential g. The mathematical expression of the plastic potential g is

$$\begin{aligned} g &= \sqrt{J_2}K_g - p' \sin\phi_d \\ &= 0, \end{aligned} \tag{22}$$

where K_g is a function for the smooth corners of the plastic potential surface. K_g has the same form as K_f; however, it depends on ϕ_d rather than ϕ_b.

3. Model Performance

The proposed model was calibrated for Toyoura sand; Table 1 lists the calibrated model parameters. The typical values of mean diameter d_{50}, maximum void ratio $e_{\max}$, and minimum void ratio $e_{\min}$ are approximately 0.19 mm, 0.977, and 0.597, respectively [24, 34–36]. Herein, the critical state angle ϕ_c was taken as 31.15° for Toyoura sand, which corresponds to $M_c = 1.25$ under triaxial compression conditions, as experimentally determined by Verdugo and Ishihara [23]. To construct the CSL of Toyoura sand, following Li et al. [37], this study set $\Gamma_{cc} = 0.934$, $\lambda = 0.019$, and $\xi = 0.7$ from triaxial compression test results. Loukidis and Salgado [14] calibrated Γ_{ce} (Γ_c under triaxial extension conditions) as 0.860, which this study follows.

For shear modulus G, this model requires the quantification of parameters C_g, α, and γ_{tv}. Following Li and Dafalias [38], Dafalias and Manzari [39], Li [16], and Li and Dafalias [40], C_g was set as 125.0 for Toyoura sand in this study. Woo et al. [7] calibrated $\alpha = 0.70$ and $\gamma_{\text{tv}} = 1.75e-4$ for Toyoura sand based on experimental data [13, 30, 41–43]; the current study uses these values for the proposed model. Poisson's ratio ν was set as 0.25 for Toyoura sand based on previous research [18, 44].

Table 1: Model parameters for Toyoura sand.

Parameters	Value	Required test
C_g	125	RC or BE/TXC
A	0.70	RC or BE
γ_{tv}	$1.75e-4$	RC or BE
N	0.25	CK_0
ϕ_{cs}	31.15°	TXC
Γ_{cc}	0.934	TXC
Γ_{ce}	0.860	TXE
λ	0.019	TXC
ξ	0.7	TXC
d_0	1.20	TXC
h_0	0.20	TXC

RC denotes the resonance column test. BE denotes the bender element test. TXC denotes the triaxial compression test. CK_0 denotes the K_0 consolidation test. TXE denotes the triaxial extension test.

Figure 2 illustrates the calibration of the dilatancy parameter d_0 (in equation (7)) using experimental data from an undrained triaxial compression test for an isotropically consolidated sand specimen (CIUTXC); a larger d_0 produces a stiffer mechanical response due to more dilatant behavior. As shown in Figure 2, d_0 was set to 1.2 for Toyoura sand. The determination of the model parameter h_0, used in calculating the hardening modulus (equation (20)), is illustrated in Figure 3; a higher h_0 yields a stiffer sand response. h_0 was calibrated against the results of a drained triaxial compression test for an isotropically consolidated sand specimen (CIDTXC) and taken as 0.2 for Toyoura sand, as shown in Figure 3.

Figures 4 and 5 plot the CIUTXC test results (hollow circles) for Toyoura sand from Verdugo and Ishihara [23], which overlap with the numerical simulation result (black line) generated by the proposed model. For comparison, the simulation results using the bounding surface M-C (BSMC) model (gray lines) with fixed dilatancy angles ϕ_d (0–10°) are plotted in the figures. These are also the simulation results from the CSMC model (black dashed line), proposed by Woo et al. [7], with identical model parameters. Figures 4(a) and 5(a) compare the stress-strain behaviors (q-ε_a curve, where ε_a represents the axial strain), whereas Figures 4(b) and 5(b) show the comparison in the p'-q space. In Figures 4(a) and 5(a), the BSMC model with a fixed ϕ_d produced significantly different stress-strain curves from the experimental results. Furthermore, shear stresses, where ϕ_d was nonzero, continually increased without stress stabilization at the critical state. The nonconvergence of stress to the critical state of the BSMC model under undrained loading is also shown in Figures 4(b) and 5(b), where both p' and q continuously increase when $\phi_d > 0$. The positive curvature of the q-ε_a curves from the BSMC model in Figures 4(a) and 5(a) is caused by the interdependence

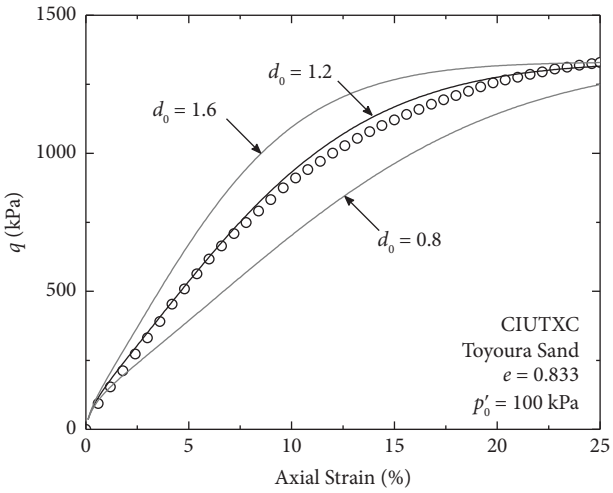

Figure 2: Calibration of d_0.

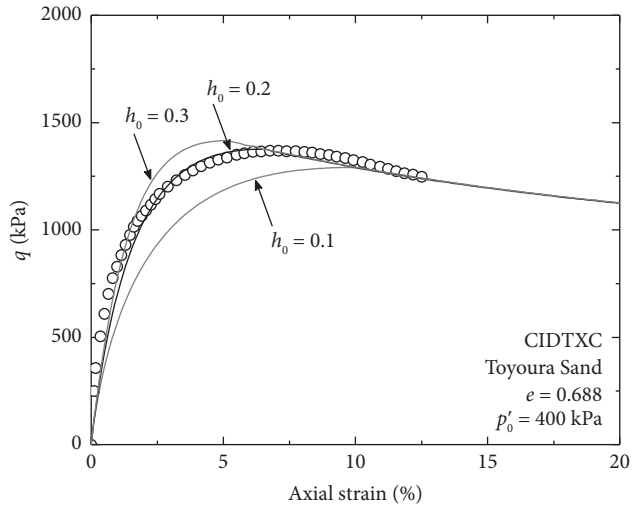

Figure 3: Calibration of h_0.

between the elastic moduli and p' throughout equations (9)–(11) for a constant ϕ_d. In contrast, both the BSCSMC and CSMC models, because ϕ_d changes during shearing and eventually vanishes at the critical state, correctly capture the mechanical response in all states, as shown in Figures 4 and 5.

Figures 6 and 7 present comparisons of the CIDTXC responses between the test data (hollow symbols) from Fukushima and Tatsuoka [45] and the simulation results (black lines) for the Toyoura sand. The initial mean effective stress p'_0 and the initial void ratio e_0 are 100 kPa and 0.824, respectively, in Figure 6, whereas $p'_0 = 400$ kPa and $e_0 = 0.688$ in Figure 7. The friction angle depends on ψ_c in the CSMC and BSCSMC models; thus, they can simulate the peak response under drained shearing within sands, as shown in Figures 6(a) and 7(a). However, CSMC predicts peaks at smaller strain levels than those in the experiment data and produces a kink at the peak and, thus, a sharp transition from elastic to plastic behavior, primarily because of the yield surface; such a sharp transition was not observed in the experimental data. On the other hand, the proposed BSCSMC model utilizes the bounding surface concept and successfully describes the smooth stress-strain responses of sand, which is in excellent agreement with the experimental results. Figures 6(b) and 7(b) show the volumetric change versus axial strain from the experimental and simulation results, respectively. Simulations (gray lines) using the BSMC model with a fixed dilatancy angle do not show a stabilization tendency of the volume change during shearing in Figures 6(b) and 7(b). On the other hand, both the BSCSMC and CSMC models show a convergence tendency of volume change during shearing.

Figure 8 presents comparisons of the CIDTXE responses between the test data from Safdar et al. [46] and the simulation results for the Toyoura sand. Figure 8(a) shows the von Mises stress q versus axial strain, whereas Figure 8(b) represents the volume change versus axial strain from the experimental data (hollow and grey symbols for $p'_0 = 50$ and 400 kPa, respectively) and simulation results (dashed and solid lines for $p'_0 = 50$ and 400 kPa, respectively). Figure 8 shows that the proposed BSCSMC model successfully describes the smooth stress-strain responses of sand, which is in good agreement with the experimental results under triaxial extension loading conditions.

3.1. Discussion. The present study compares the BSCSMC model with the SANISAND (or two-surface) models, originated by Manzari and Dafalias [12], and the Norsand model, originally proposed by Jefferies [47], which have successfully described the mechanical responses of sand. For the SANISAND and Norsand models, this paper selected the models proposed by Li and Dafalias [38] and Boukpeti et al. [48], respectively, which presented both triaxial compression and extension simulation results. Generally, the difficulty of a calibration step of a constitutive model is proportional to the number of parameters determined by the trial-and-error method. Model parameters of soil constitutive models based on the critical state framework can be classified into parameter groups used in the construction of elastic moduli, critical state surface in the stress space, critical state line in the plane of void ratio (or specific volume), mean effective stress, and plasticity formulation. Among the parameter groups, parameters related to the plasticity formulation (flow, hardening, and evolution rules) generally require the trial-and-error method for the calibration. Table 2 lists the number of model parameters in each parameter group for SANISAND [38], Norsand [48], and the proposed model. For the plasticity formulation, SANISAND [38] and Norsand [48] require 10 and 6 parameters, respectively, whereas the proposed BSCSMC model requires only two parameters (h_0 and d_0); thus, the calibration step in the proposed model needs less efforts than the SANISAND and Norsand models.

Realistically, the experimental data show contractive behavior (reduction of e) before the phase transformation point; thereafter, the sands begin to dilate (increase of e).

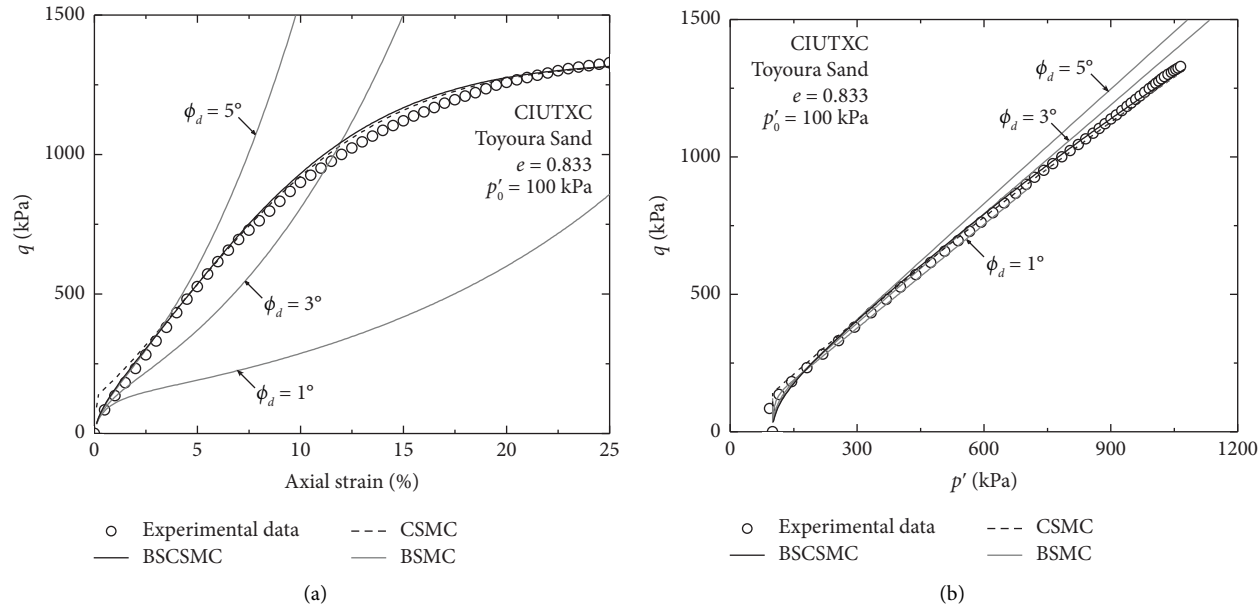

Figure 4: CIUTXC test results from Verdugo and Ishihara [23] and simulated results (BSCSMC) for Toyoura sand ($e = 0.833$; $p'_0 = 100$ kPa). The simulation results from the bounding surface M-C model (BSMC) with fixed dilatancy angles ϕ_d and the CSMC model [7] are plotted for comparison: (a) axial strain vs. q and (b) p' vs. q.

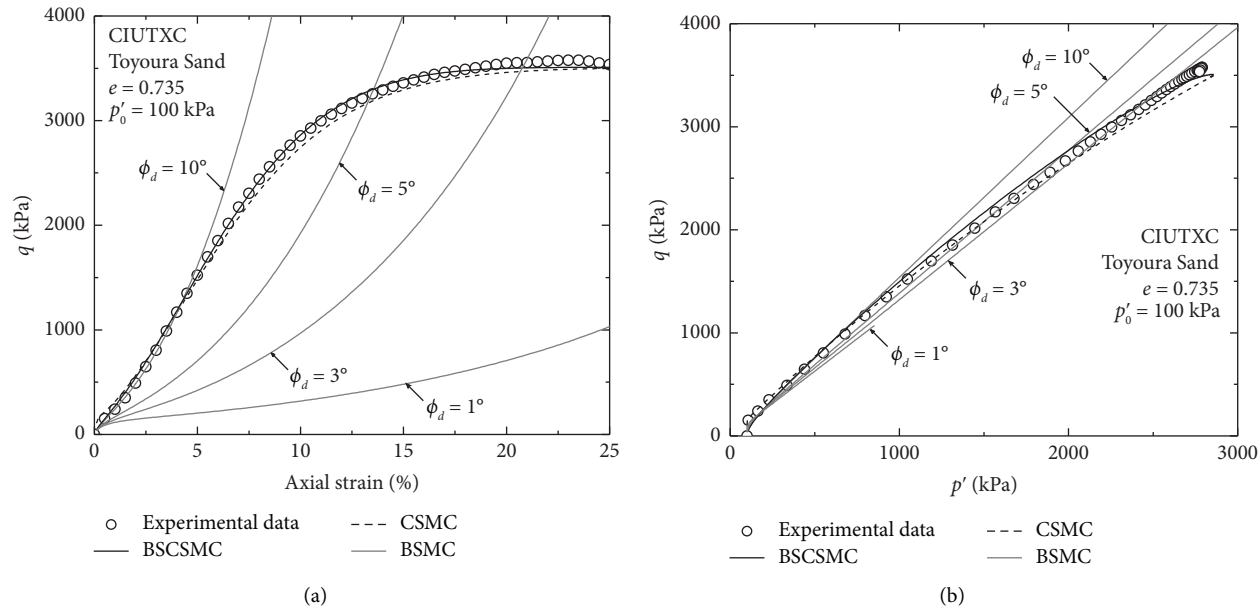

Figure 5: CIUTXC test results from Verdugo and Ishihara [23] and simulated results (BSCSMC) for Toyoura sand ($e = 0.735$; $p'_0 = 100$ kPa). The simulation results from the bounding surface M-C model (BSMC) with fixed dilatancy angles ϕ_d and the CSMC model [7] are plotted for comparison: (a) axial strain vs. q and (b) p' vs. q.

Because the proposed BSCSMC model does not include a formulation to describe the phase transformation point, there are slight differences between experimental and simulation results. This is the main disadvantage of the proposed model compared to the SANISAND and Norsand models. However, this contractive phase before the phase

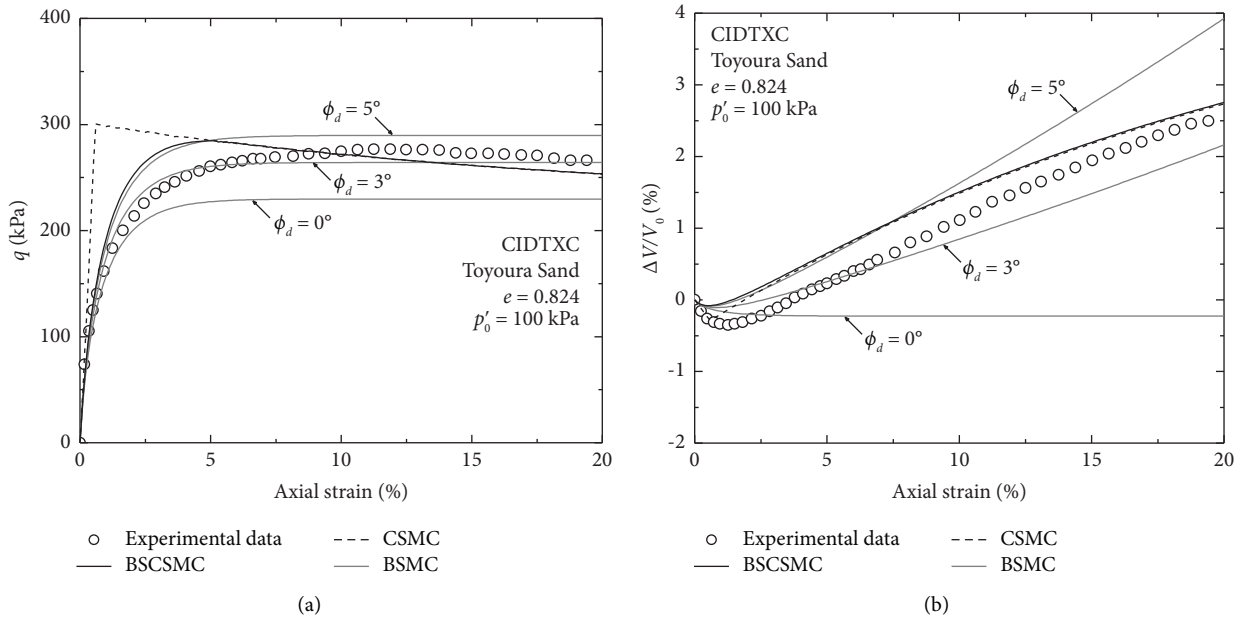

Figure 6: CIDTXC test results from Fukushima and Tatsuoka [45] and simulated results (BSCSMC) for Toyoura sand ($e_0 = 0.824$; $p'_0 = 100$ kPa). The simulation results from the bounding surface M-C model (BSMC) with fixed dilatancy angles ϕ_d and the CSMC model [7] are plotted for comparison: (a) axial strain vs. q and (b) axial strain vs. volume change $\Delta V/V_0$.

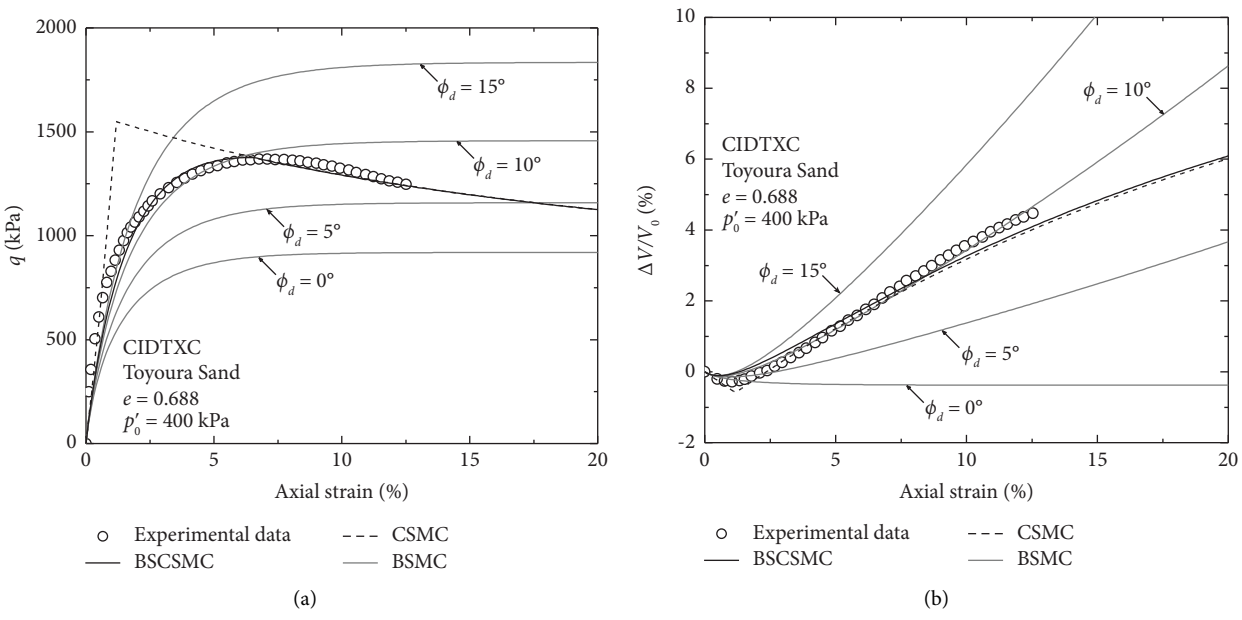

Figure 7: CIDTXC test results from Fukushima and Tatsuoka [45] and simulated results (BSCSMC) for Toyoura sand ($e_0 = 0.688$; $p'_0 = 400$ kPa). The simulation results from the bounding surface M-C model (BSMC) with fixed dilatancy angles ϕ_d and the CSMC model [7] are plotted for comparison: (a) axial strain vs. q and (b) axial strain vs. volume change $\Delta V/V_0$.

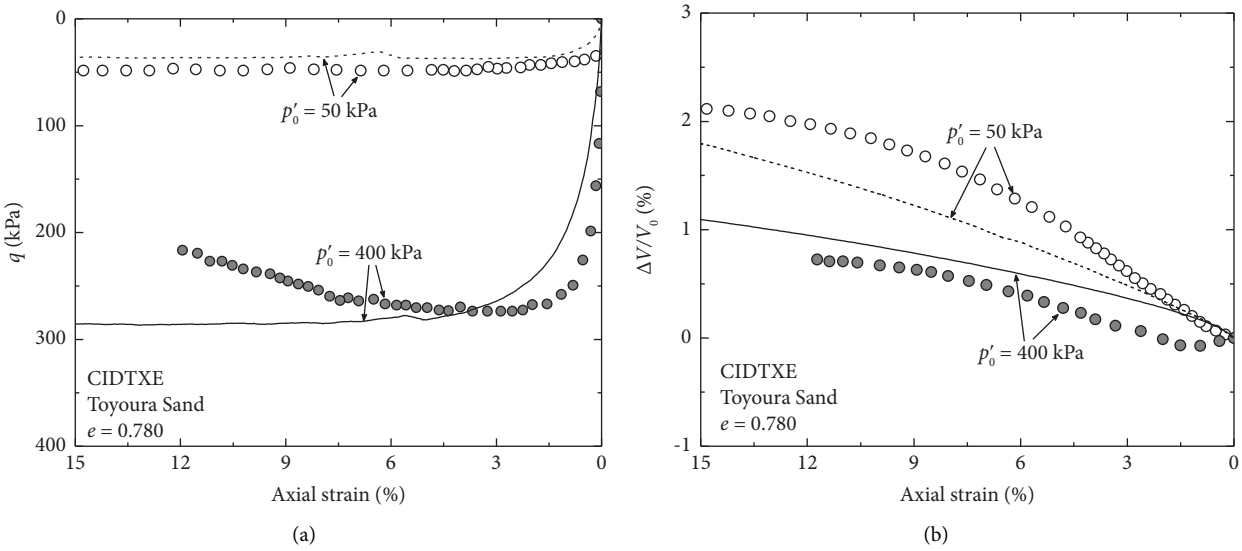

Figure 8: CIDTXE test results (symbols) from [46] and BSCSMC-simulated results (lines) for Toyoura sand ($e_0 = 0.780$): (a) axial strain vs. q and (b) axial strain vs. volume change $\Delta V/V_0$.

Table 2: Number of model parameters required in SANISAND [38], Norsand [48], and the proposed model.

No. parameter	SANISAND [38]	Norsand [48]	BSCSMC (this study)
Elastic moduli	2	2	4
Critical state surface in the stress space	2	1	1
Critical state line in the e-p' plane	3	2	4
Plasticity formulation (flow, hardening, and evolution rules)	10	6	2
Total	17	11	11

transformation point can be described by applying the dilatancy surface concept [12] or phase transformation line [15] to the present model.

4. Conclusions

This paper proposes a BSCSMC model for sands. The BSCSMC model used the smoothed M-C failure surface as its bounding surface, rather than the yield surface, to describe the smooth transition from elastic to plastic behavior. This model sets the dilatancy and friction angles, which are conventionally assumed to be constants, as functions of the state parameter, which represents the distance to the critical state. Therefore, the proposed model could describe the peak response for dense sands and the stress stabilization of sands at the critical state.

The BSCSMC model can simulate the undrained and drained triaxial compression behaviors of Toyoura sand better than the bounding surface M-C model, with a fixed dilatancy angle, and the CSMC model. The proposed BSCSMC model numerically described the complex mechanical responses of sands, including the smooth stress-strain response, peak behavior, and the critical state, under both undrained and drained conditions.

Data Availability

The data supporting the findings of this study are available from the corresponding author upon request.

Conflicts of Interest

The author declares that there are no conflicts of interest.

Acknowledgments

This work was supported by the Incheon National University Research Grant in 2022.

References

[1] B. Yuan, Z. Li, Y. Chen et al., "Mechanical and microstructural properties of recycling granite residual soil reinforced with glass fiber and liquid-modified polyvinyl alcohol polymer," *Chemosphere*, vol. 286, Article ID 131652, 2022.

[2] C. S. Tang, D.-Y. Wang, Y. J. Cui, B. Shi, and J. Li, "Tensile strength of fiber-reinforced soil," *Journal of Materials in Civil Engineering*, vol. 28, no. 7, 2016.

[3] B. Yuan, Z. Li, W. Chen et al., "Influence of groundwater depth on pile–soil mechanical properties and fractal characteristics under cyclic loading," *Fractal and Fractional*, vol. 6, pp. 198–204, 2022.

[4] C. H. C. Tsuha, P. Y. Foray, R. J. Jardine, Z. X. Yang, M. Silva, and S. Rimoy, "Behaviour of displacement piles in sand under cyclic axial loading," *Soils and Foundations*, vol. 52, no. 3, pp. 393–410, 2012.

[5] B. Bai, R. Zhou, G. Cai, W. Hu, and G. Yang, "Coupled thermo-hydro-mechanical mechanism in view of the soil particle rearrangement of granular thermodynamics," *Computers and Geotechnics*, vol. 137, Article ID 104272, 2021.

[6] B. Bai, G. Yang, T. Li, and G. Yang, "A thermodynamic constitutive model with temperature effect based on particle rearrangement for geomaterials," *Mechanics of Materials*, vol. 139, Article ID 103180, 2019.

[7] S. I. Woo, H. Seo, and J. Kim, "Critical-state-based Mohr-Coulomb plasticity model for sands," *Computers and Geotechnics*, vol. 92, pp. 179–185, 2017.

[8] K. Been and M. G. Jefferies, "A state parameter for sands," *Géotechnique*, vol. 35, no. 2, pp. 99–112, 1985.

[9] A. Casagrande, "Characteristics of Cohesionless Soils Affecting the Stability of Slopes and Earth Fills," *Journal of the Boston Society of Civil Engineers*, vol. 23, no. 1, pp. 13–32, 1936.

[10] M. D. Bolton, "The strength and dilatancy of sands," *Géotechnique*, vol. 36, no. 1, pp. 65–78, 1986.

[11] D. M. Wood, K. Belkheir, and D. F. Liu, "Strain softening and state parameter for sand modelling," *Géotechnique*, vol. 44, no. 2, pp. 335–339, 1994.

[12] M. T. Manzari and Y. F. Dafalias, "A critical state two-surface plasticity model for sands," *Géotechnique*, vol. 47, no. 2, pp. 255–272, 1997.

[13] A. G. Papadimitriou, G. D. Bouckovalas, and Y. F. Dafalias, "Plasticity model for sand under small and large cyclic strains," *Journal of Geotechnical and Geoenvironmental Engineering*, vol. 127, no. 11, pp. 973–983, 2001.

[14] D. Loukidis and R. Salgado, "Modeling sand response using two-surface plasticity," *Computers and Geotechnics*, vol. 36, no. 1-2, pp. 166–186, 2009.

[15] S. I. Woo and R. Salgado, "Bounding surface modeling of sand with consideration of fabric and its evolution during monotonic shearing," *International Journal of Solids and Structures*, vol. 63, pp. 277–288, 2015.

[16] X. S. Li, "A sand model with state-dependent dilatancy," *Géotechnique*, vol. 52, no. 3, pp. 173–186, 2002.

[17] Z. Wang, Y. F. Dafalias, C. Shen, and C. K. Shen, "Bounding surface hypoplasticity model for sand," *Journal of Engineering Mechanics*, vol. 116, no. 5, pp. 983–1001, 1990.

[18] X. S. Li and Y. F. Dafalias, "A constitutive framework for anisotropic sand including non-proportional loading," *Géotechnique*, vol. 54, no. 1, pp. 41–55, 2004.

[19] A. Lashkari and M. S. Yaghtin, "Sand flow liquefaction instability under shear–volume coupled strain paths," *Géotechnique*, vol. 68, no. 11, pp. 1002–1024, 2018.

[20] Z. Gao and J. Zhao, "A non-coaxial critical-state model for sand accounting for fabric anisotropy and fabric evolution," *International Journal of Solids and Structures*, vol. 106-107, no. 107, pp. 200–212, 2017.

[21] K. H. Roscoe, A. N. Schofield, and C. P. Wroth, "On the yielding of soils," *Géotechnique*, vol. 8, no. 1, pp. 22–53, 1958.

[22] X. S. Li, "Modeling of dilative shear failure," *Journal of Geotechnical and Geoenvironmental Engineering*, vol. 123, no. 7, pp. 609–616, 1997.

[23] R. Verdugo and K. Ishihara, "The steady state of sandy soils," *The steady state of sandy soils: Soils and Foundations*, vol. 36, no. 2, pp. 81–91, 1996.

[24] M. Yoshimine, P. K. Robertson, and C. E. Fear Wride, "Undrained shear strength of clean sands to trigger flow liquefaction," *Canadian Geotechnical Journal*, vol. 36, no. 5, pp. 891–906, 1999.

[25] A. Lashkari, "On the modeling of the state dependency of granular soils," *Computers and Geotechnics*, vol. 36, no. 7, pp. 1237–1245, 2009.

[26] X. Tu, J. E. Andrade, and Q. Chen, "Return mapping for nonsmooth and multiscale elastoplasticity," *Computer Methods in Applied Mechanics and Engineering*, vol. 198, no. 30-32, pp. 2286–2296, 2009.

[27] Q. Chen, J. E. Andrade, and E. Samaniego, "AES for multiscale localization modeling in granular media," *Computer Methods in Applied Mechanics and Engineering*, vol. 200, no. 33-36, pp. 2473–2482, 2011.

[28] F. Richart, J. Hall, and R. Woods, *Vibrations of Soils and Foundations*, Prentice-Hall, Englewood Cliffs, NJ, USA, 1970.

[29] K. I. Andrianopoulos, A. G. Papadimitriou, and G. D. Bouckovalas, "Bounding surface plasticity model for the seismic liquefaction analysis of geostructures," *Soil Dynamics and Earthquake Engineering*, vol. 30, no. 10, pp. 895–911, 2010.

[30] A. G. Papadimitriou and G. D. Bouckovalas, "Plasticity model for sand under small and large cyclic strains: a multiaxial formulation," *Soil Dynamics and Earthquake Engineering*, vol. 22, no. 3, pp. 191–204, 2002.

[31] I. Einav, A. M. Puzrin, and A. M. Asce, "Pressure-dependent elasticity and energy conservation in elastoplastic models for soils," *Journal of Geotechnical and Geoenvironmental Engineering*, vol. 130, no. 1, pp. 81–92, 2004.

[32] A. Lashkari and A. Golchin, "On the influence of elastic-plastic coupling on sands response," *Computers and Geotechnics*, vol. 55, pp. 352–364, 2014.

[33] A. J. Abbo, *Finite Element Algorithms for Elastoplasticity and Consolidation*, University of Newcastle, Callaghan, Australia, 1997.

[34] M. Yoshimine, K. Ishihara, and W. Vargas, "Effects of principal stress direction and intermediate principal stress on undrained shear behavior of sand," *Soils and Foundations*, vol. 38, no. 3, pp. 179–188, 1998.

[35] M. Yoshimine and M. Kataoka, "Steady State of Sand in Triaxial Extension test," *International Workshop On Earthquake Hazards And Mitigation*, I. K. International Pvt Ltd, New Delhi, India, 2007.

[36] Y. Hosono and M. Yoshimine, "Liquefaction of sand in simple shear condition," *Cyclic behaviour of soils and liquefaction phenomena*, pp. 129–136, Ruhr University Bochum, Bochum, Germany, 2004.

[37] X. S. Li, Y. F. Dafalias, and Z. L. Wang, "State-dependant dilatancy in critical-state constitutive modelling of sand," *Canadian Geotechnical Journal*, vol. 36, no. 4, pp. 599–611, 1999.

[38] X. S. Li and Y. F. Dafalias, "Anisotropic critical state theory: role of fabric," *Journal of Engineering Mechanics*, vol. 138, no. 3, pp. 263–275, 2012.

[39] Y. F. Dafalias and M. T. Manzari, "Simple plasticity sand model accounting for fabric change effects," *Journal of Engineering Mechanics*, vol. 130, no. 6, pp. 622–634, 2004.

[40] X. S. Li and Y. F. Dafalias, "Dilatancy for cohesionless soils," *Géotechnique*, vol. 50, no. 4, pp. 449–460, 2000.

[41] M. Vucetic, "Cyclic threshold shear strains in soils," *Journal of Geotechnical Engineering*, vol. 120, no. 12, pp. 2208–2228, 1994.

[42] R. C. Gomes, J. A. Santos, A. Modaressi-Farahmand Razavi, and F. Lopez-Caballero, "Validation of a strategy to predict secant shear modulus and damping of soils with an elasto-plastic model," *KSCE Journal of Civil Engineering*, vol. 20, no. 2, pp. 609–622, 2016.

[43] D. Kim and Y. W. Choo, "Cyclic threshold shear strains of sands based on pore water pressure buildup and variation of deformation characteristics," *International Journal of Offshore and Polar Engineering*, vol. 16, no. 1, pp. 57–64, 2006.

[44] X. S. Li and Y. F. Dafalias, "Constitutive modeling of inherently anisotropic sand behavior," *Journal of Geotechnical and Geoenvironmental Engineering*, vol. 128, no. 10, pp. 868–880, 2002.
[45] S. Fukushima and F. Tatsuoka, "Strength and deformation characteristics of saturated sand at extremely low pressures," *Soils and Foundations*, vol. 24, no. 4, pp. 30–48, 1984.
[46] M. Safdar, T. Newson, and F. Shah, "Consolidated drained (CID) behavior of fibre reinforced cemented Toyoura sand in triaxial loading conditions," *International Journal of Geo-Engineering*, vol. 12, no. 1, p. 27, 2021.
[47] M. G. Jefferies, "Nor-Sand: a simple critical state model for sand," *Géotechnique*, vol. 43, no. 1, pp. 91–103, 1993.
[48] N. Boukpeti, Z. Mróz, and A. Drescher, "A model for static liquefaction in triaxial compression and extension," *Canadian Geotechnical Journal*, vol. 39, no. 6, pp. 1243–1253, 2002.